


## Research Article

# Electrochemical, Isotherm, and Material Strength Studies of *Cucumeropsis mannii* Shell Extract on A515 Grade 70 Carbon Steel in NaCl Solution

Lekan Taofeek Popoola <sup>1</sup>, Adeyinka Sikiru Yusuff,<sup>1</sup> Omolayo Michael Ikumapayi,<sup>2</sup> Onyemaechi Melford Chima,<sup>3</sup> Adebayo Tajudeen Ogunyemi,<sup>1</sup> and Babatunde Adegoke Obende<sup>4</sup>

<sup>1</sup>Chemical and Petroleum Engineering Department, Afe Babalola University, Ado-Ekiti, Ekiti State, Nigeria

<sup>2</sup>Mechanical and Mechatronics Engineering Department, Afe Babalola University, Ado-Ekiti, Ekiti State, Nigeria

<sup>3</sup>Mechanical Engineering Department, Michael Okpara University of Agriculture, Umudike, Abia State, Nigeria

<sup>4</sup>Civil Engineering Department, Afe Babalola University, Ado-Ekiti, Ekiti State, Nigeria

Correspondence should be addressed to Lekan Taofeek Popoola; [popoolalekantaofeek@yahoo.com](mailto:popoolalekantaofeek@yahoo.com)

Received 5 July 2022; Revised 15 July 2022; Accepted 18 July 2022; Published 29 July 2022

Academic Editor: Michael J. Schütze

Copyright © 2022 Lekan Taofeek Popoola et al. This is an open access article distributed under the Creative Commons Attribution License, which permits unrestricted use, distribution, and reproduction in any medium, provided the original work is properly cited.

In this study, corrosion inhibition efficiency of *Cucumeropsis mannii* shell extract (CMSE) was tested on A515 Grade 70 carbon steel in 1.0 M NaCl solution. Potentiodynamic polarization (PDP), electrochemical impedance spectroscopy (EIS), and weight loss (WL) measurements were used to investigate the inhibition efficiency. Scanning electron microscopy, Fourier transform infrared spectroscopy, atomic adsorption spectroscopy, and energy dispersive spectroscopy were used to characterize the carbon steel and extract. PDP and EIS measurements revealed maximum inhibition efficiency of 91.2% and 92.2%, respectively. Tafel plot confirmed inhibitor to be a mixed type. A monolayer adsorption of CMSE molecules occurred spontaneously by physisorption. Polarization resistance increased with increasing inhibitor concentration. WL measurement revealed decrease in corrosion rate with increasing concentration of corrosion inhibitor. Maximum Young modulus and hardness of 202.4 GPa and 112.3 BHN, respectively, were recorded for the carbon steel at a minimum corrosion rate and load. Pitting and uniform corrosion were formed on the carbon steel in the absence of CMSE. CMSE contains  $-OH$ ,  $-OCH_3$ , and  $-C-NH_3$  as active functional groups. In conclusion, *Cucumeropsis mannii* shell extract acted excellently as corrosion inhibitor for A515 Grade 70 carbon steel in 1.0 M NaCl.

## 1. Introduction

Materials quality tends to decrease due to their chemical reaction with other elements found in natural (dry and wet) environments [1]. This is generally termed corrosion, whose rate is majorly a function of time, temperature, and concentration of reactant [2]. Literatures have proved investigation of carbon steel corrosion inhibition as the most common because of its low-cost, relatively high strength,

availability, and numerous industrial applications [3]. Carbon steel accounts for approximately 85% of annual steel production worldwide and is the most widely used structural engineering material [4]. It has found the widest application in construction, power plants, marine, petroleum refining and production, chemical processing, and so on [5]. Nonetheless, sodium chloride is a multipurpose salt having practically unlimited industrial applications. It serves as a flocculant for drilling fluids in oil and gas industries to

increase their density and lower downwell gas pressures. Also, it is often injected to enhance solution saturation when salt formation is noticed during drilling [6]. In textile industries during dyeing operation, sodium chloride serves as a brine rinse to improve salting out of precipitates formed [7]. In mining industries, it is used in processing copper, aluminum, vanadium, beryllium, and steel. However, carbon steel is severely corroded when in contact with sodium chloride solution during the aforementioned operations [8]. The use of corrosion inhibitors was the best approach to protect metals against corrosion [9]. The mechanisms involve adsorption onto metal surfaces, formation of thick films, and blockage of active sites and thereby decrease in corrosion rate [10]. However, extracts of natural plant origin have proved to be inexpensive, environmentally, and ecofriendly safe corrosion inhibitors [8, 11, 12]. Anticorrosion efficiency of extracts from *Asafoetida* [13], *Myrmecodia pendans* [14], *Ricinus communis* [15], terebinth [16], *Artemisia* [17], and peach pomace [18] on carbon steel in chloride medium has been previously investigated.

The influence of corrosion inhibitors on the mechanical properties of metals is vital. Only few studies examined carbon steel strength in the presence and absence of these corrosion inhibitors in chloride solution [19, 20]. Investigating the behavior of structural materials via material testing is crucial. Tensile test is a major one which predicts the quantity of stress the materials can withstand under excessive deformation or fracture and thus their suitability for structural applications. Previously, Guo et al. [21] investigated Q235 steel corrosion in  $H_2SO_4$  medium using 3,3-dithiodipropionic acid (DDA) as a potential corrosion inhibitor. Also, Tan et al. [22] used a simple and green pure water extraction method to obtain extract from *Passiflora edulia* Sims leaves and used it as corrosion inhibitor for copper in sulfuric acid solution. In this study, tensile test was conducted for A515 Grade 70 carbon steel subjected to corrosion in 1.0 M NaCl using *Cucumeropsis mannii* shell extract (CMSE) as corrosion inhibitor. The mechanical properties were obtained in the presence and absence of CMSE. The presence of phenolic compounds (containing –OH and –OCH<sub>3</sub> as polar functional groups) such as flavonoids, phytosterols, and tocopherols in *Cucumeropsis mannii* shell enhance its suitability as corrosion inhibitor for carbon steel in sodium chloride solution [23]. They acted as adsorption sites when their electron-releasing substituents are attached on metal surface via  $\pi$ - and nonbonding electrons and thus prevent corrosion by forming thin films [12]. The corrosion inhibitor efficiency was measured by potentiodynamic polarization (PDP), electrochemical impedance spectroscopy (EIS), and weight loss (WL) methods. Central composite design (CCD) of Design-Expert 7.0.0 was adopted for experimental design at different temperature ( $T$ ), immersion time ( $t$ ), inhibitor concentration ( $C$ ), and load ( $L$ ). The adsorption behavior of CMSE molecules on A515 Grade 70 carbon steel in the chloride solution was studied using Langmuir adsorption isotherm and Gibb's free energy. Scanning electron microscopy, Fourier transform infrared spectroscopy, atomic adsorption spectroscopy, and energy dispersive spectroscopy were used to characterize the carbon steel and extract.

TABLE 1: Chemical composition of A515 Grade 70 carbon steel sample.

Element	Fe	C	Mn	P	Si	S
Composition (%)	98.00	0.35	1.2	0.035	0.375	0.04

## 2. Materials and Methods

**2.1. Sample Preparation.** Table 1 presents the composition of A515 Grade 70 carbon steel used. Carbon steel of 6 mm thick was cut into coupons of equal dimension (6 cm  $\times$  4 cm) having exposed surface areas of 24 cm<sup>2</sup>. Samples were smoothly polished using different grades of SiC paper that were used to polish the samples while ethanol and acetone were used for degreasing and drying, respectively. Samples were then stored in a desiccator for the weight loss method.

**2.2. Preparation of Corrosion Inhibitor.** Shells of *Cucumeropsis mannii* (CMS) were hand-picked, mechanically grinded into fine particles (63  $\mu$ m), and stored in a covered plastic. About 100 g of CMS was dissolved in 1000 mL of ethanol for 48 hours. Whatman filter paper was used to separate the filtrate from the residue. Ethanol was removed from the filtrate by heating at a temperature of 80°C and was stocked. Different concentrations of corrosion inhibitor were prepared from the stock solution by dissolving 2, 6, and 10 g of extract in 1 L of 1.0 M NaCl, respectively.

**2.3. Corrosive Medium Preparation.** The corrosive medium was a saline solution of 1.0 M NaCl. It was prepared by dissolving sodium chloride crystals (analytical grade) in distilled water.

**2.4. Electrochemical Measurements.** A three-electrode electrochemical cell consisting saturated calomel (reference electrode), graphite rod (counter electrode), and 1 cm<sup>2</sup> A515 Grade 70 CS coupons (working electrode) was employed to measure the results of electrochemical methods. The corrosion cell was connected to a computer-controlled 263 galvanostat/potentiostat electrochemical workstation. In order to ensure steady state was achieved, the working electrode was submerged for one hour in naturally aerated and unstirred solution at a constant temperature of 30  $\pm$  1°C. Impedance measurements were taken at 5 mV perturbation signal amplitude and 100 kHz to 10 MHz frequency range for corrosion potentials ( $E_{\text{corr}}$ ). Polarization studies were examined in the range -0.8 V to -0.2 V versus corrosion potential at a scan rate of 0.333 mV/s. Equation Equation (1) was used to calculate the percentage inhibition efficiency (IE%).

$$IE_p \% = \left( \frac{i_{\text{corr}(\text{bl})} - i_{\text{corr}(\text{inh})}}{i_{\text{corr}(\text{bl})}} \right) \times 100\%, \quad (1)$$

where  $i_{\text{corr}(\text{bl})}$  and  $i_{\text{corr}(\text{inh})}$  are respective values of corrosion current densities in the absence and presence of corrosion inhibitor.

TABLE 2: Factors and values at two levels for batch corrosion experiments.

Independent variables	Factor	Unit	Values of coded levels	
			-1	+1
Temperature ( $T$ )	$X_1$	$^{\circ}\text{C}$	30.0	60.0
Immersion time ( $t$ )	$X_2$	Day	1.0	5.0
Inhibitor concentration ( $C$ )	$X_3$	$\text{gL}^{-1}$	2	10
Load ( $L$ )	$X_4$	$N$	15,000	30,000

**2.5. Corrosion Rate Determination Using Weight Loss Method.** The weight loss method was adopted to determine the corrosion rate of carbon steel in 1.0 M NaCl solution in the presence and absence of CMSE at varying temperature and time. In the presence of CMSE, the corrosion rate was determined at varying inhibitor concentration. For each experiment, a digital weighing balance was used to weigh carbon steel coupons after immersion in 50 mL of 1.0 M NaCl in the presence and absence of varying CMSE concentrations. Before this, samples were washed using distilled water and acetone and were dried using a clean cloth. The corrosion rate was calculated using Equation (2).

$$\text{CR}(\text{mm/y}) = \frac{87,500W}{A\rho t}, \quad (2)$$

where CR is the corrosion rate (mm/y),  $W$  is the weight loss (g),  $A$  is the carbon steel coupon area ( $\text{cm}^2$ ),  $\rho$  is the density ( $\text{g/cm}^3$ ), and  $t$  is the immersion time (hr).

**2.6. Tensile Test for Carbon Steel Mechanical Properties.** The tensile test was conducted in accordance with ASTM E-8 standard using a Universal Testing Machine (Hi-Tech, HSM58i) to determine Young modulus of carbon steel in the corrosive medium in the presence and absence of CMSE. Carbon steel surface hardness was determined using a Rockwell Hardness Tester TH 550. The load was varied between 15,000 N to 30,000 N.

**2.7. Design of Experiments.** The effects of temperature, immersion time, and inhibitor concentration were investigated on the corrosion rate of carbon steel in sodium chloride under the influence of CMSE as corrosion inhibitor. Young modulus and hardness of A515 Grade 70 CS coupons were measured considering load between 15,000 to 30,000 N. The parameters were varied at two different levels as shown in Table 2 with a total of 30 experiments using central composite design (CCD) of Design-Expert 7.0.0. The responses were corrosion rate, Young modulus, and hardness.

**2.8. Material Characterization.** Functional groups in CMSE were detected using Fourier transform infrared spectrophotometer (Nicolet iS10). Scanning electron microscope (SEM/EDX-JEOL-JSM 7600F) was used for carbon steel surface morphology examination with and without CMSE. Energy dispersive spectroscopy, an attached accessory to scanning electron microscope, was used for detecting elemental percentages on carbon

steel surface in the presence and absence of CMSE. The concentration of  $\text{Fe}^{2+}$  loss into the corrosive medium was checked using atomic adsorption spectroscopy.

### 3. Results and Discussions

#### 3.1. Electrochemical Measurements

**3.1.1. Potentiodynamic Polarization Measurements.** Figure 1 presents the potentiodynamic polarization curve indicating the effect of CMSE on the electrochemical behavior of A515 Grade 70 carbon steel in 1 M NaCl solution at 303 K. This was examined between -0.8 V and -0.2 V [24]. Tafel straight line extrapolation was used to obtain values of corrosion current density ( $i_{\text{corr}}$ ), corrosion potential ( $E_{\text{corr}}$ ), anodic ( $\beta_a$ ), and cathodic ( $\beta_c$ ) Tafel slopes and percent inhibition efficiency (IE%) presented in Table 3. The result revealed preservation of carbon steel surface by protective layers of CMSE because  $i_{\text{corr}}$  values decreased when inhibitor concentrations were increased [25]. This is supported by the increased in the inhibition efficiency as the inhibitor concentrations were increased. A maximum value of 91.2% was reached. Furthermore, a more noble corrosion potential was observed with decreased in  $\beta_a$  and  $\beta_c$  values on adding CMSE to the solution. However, the anodic Tafel slope value decreased significantly suggesting that iron oxidation reaction mechanism was influenced [24]. The small change in cathodic Tafel slope value suggested adsorbed compounds of CMSE on A515 Grade 70 carbon steel did not strongly influence cathodic hydrogen evolution mechanism but rather blocked the active sites [26]. Also, the  $E_{\text{corr}}$  values were observed to shift towards the anodic potential with the change to be less than  $\pm 85$  mV. This suggested CMSE to be a mixed-type inhibitor with high prevalence at the anodic site [9].

**3.1.2. Electrochemical Impedance Spectroscopy (EIS) Measurements.** Figure 2 represents the impedance Nyquist curves of A515 Grade 70 carbon steel samples in 1 M NaCl solution in the presence and absence of different concentrations of CMSE. The observed increase in capacitive arc radius as the concentration of CMSE increases reflects improvement in the corrosion resistance of the carbon steel [27]. The observed imperfect semicircles of various diameters in all samples could be linked to frequency dispersion as a result of corrosion-induced nonhomogeneity of the carbon steel surface. Also, the capacitive arc shape can be affected by surface heterogeneity caused by increase in adsorption of organic constituents of CMSE on metal interfaces [28].

Figure 3 shows the adopted equivalent electrical circuit for examining the impedance spectra. It is made up of solution resistance ( $R_s$ ), polarization resistance ( $R_{\text{ct}}$ ), and constant phase element (CPE).

Equation (3) expresses the impedance of CPE ( $Z_{\text{CPE}}$ ) [29].

$$Z_{\text{CPE}} = \frac{1}{(Y_o)(j\omega)^n}, \quad (3)$$

where  $\omega$  is the angular frequency ( $\text{rads}^{-1}$ ),  $n$  is the phase shift (measures surface inhomogeneity and value could be  $\frac{1}{2}$ , 1, 0,

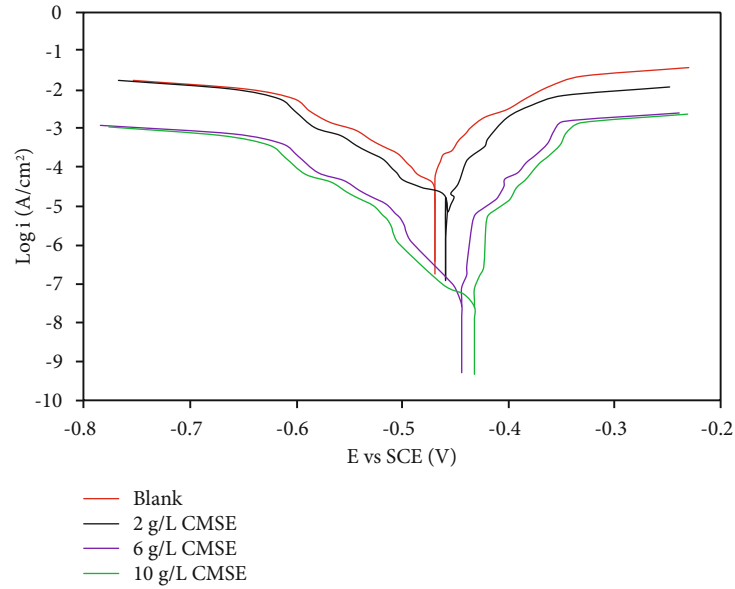


FIGURE 1: The effect of various CMSE concentrations on the electrochemical behavior of A515 Grade 70 carbon steel in 1 M NaCl solution at 303 K.

TABLE 3: Polarization parameters and corrosion inhibition efficiency of A515 Grade 70 carbon steel in 1 M NaCl solution at 303 K in the absence and presence of various concentrations of CMSE.

Conc. (g/L)	$\beta_a$ (mV)	$-\beta_c$ (mV)	$i_{corr}$ ( $\mu\text{A cm}^{-2}$ )	$E_{corr}$ (mV)	$IE_p$ (%)
Blank	$109.56 \pm 3.1$	$126.42 \pm 5.9$	$103.41 \pm 2.1$	$-489.26 \pm 0.01$	—
2	$64.18 \pm 2.6$	$112.46 \pm 4.4$	$33.72 \pm 1.5$	$-452.33 \pm 0.05$	67.4
6	$58.74 \pm 1.8$	$131.55 \pm 4.1$	$22.46 \pm 1.9$	$-438.95 \pm 0.05$	78.3
10	$47.06 \pm 1.4$	$115.75 \pm 3.8$	$9.12 \pm 0.3$	$-427.06 \pm 0.03$	91.2

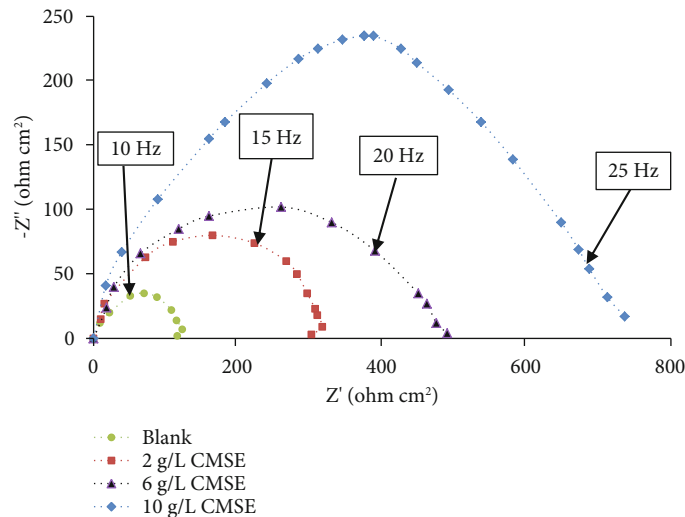


FIGURE 2: Nyquist plots of carbon steel in in 1 M NaCl solution at 303 K in the absence and presence of various concentrations of CMSE.

and  $-1$  for Warburg impedance, pure capacitance, resistance, and inductance, respectively), is the CPE constant, and  $j$  is the imaginary number ( $j^2 = -1$ ).

Equation (4) expresses the electrical double layer capacitance ( $C_{dl}$ ) calculated using CPE magnitude, polarization resistance ( $R_{ct}$ ), and phase shift  $n$  while Equation (5)

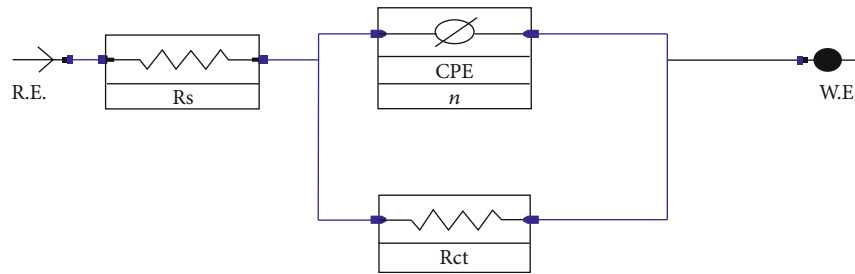


FIGURE 3: Adopted equivalent circuit model for assessing the results of electrochemical impedance spectroscopy.

TABLE 4: EIS parameters and corrosion inhibition efficiency of A515 Grade 70 carbon steel in 1 M NaCl solution at 303 K in the absence and presence of various concentrations of CMSE.

Conc. (g/L)	$R_s$ ( $\Omega\text{cm}^2$ )	$R_{ct}$ ( $\Omega\text{cm}^2$ )	$Y_o$ ( $\Omega^{-1} \text{s}^n \text{cm}^{-1}$ ) $\times 10^4$	$n$	$C_{dl}$ ( $\mu\text{F cm}^{-2}$ )	$IE_E$ (%)
Blank	$0.68 \pm 0.01$	$16.4 \pm 1.1$	$5.79 \pm 0.09$	$0.841 \pm 0.03$	$173.7 \pm 8.3$	—
2	$2.31 \pm 0.05$	$61.8 \pm 3.6$	$3.25 \pm 0.06$	$0.847 \pm 0.01$	$124.6 \pm 6.8$	73.5
6	$4.25 \pm 0.09$	$128.3 \pm 8.5$	$1.81 \pm 0.02$	$0.853 \pm 0.01$	$53.9 \pm 4.6$	87.2
10	$2.81 \pm 0.03$	$211.6 \pm 13.9$	$1.29 \pm 0.01$	$0.838 \pm 0.04$	$48.1 \pm 3.7$	92.2

TABLE 5: Langmuir isotherm parameters.

$C$ (g/L)	$IE_E$ (%)	$\theta$	$C/\theta$	$\text{Log}(C/\theta)$	$\text{Log } C$
2	73.5	0.735	2.722	0.435	0.301
6	87.2	0.872	6.879	0.838	0.778
10	92.2	0.922	10.840	1.035	1.000

expresses the inhibition efficiency calculated from polarization resistance in the absence ( $R_{ct(\text{bl})}$ ) and presence ( $R_{ct(\text{inh})}$ ) of CMSE [30].

$$C_{dl} = \left( Y_o^{1/n} R_{ct}^{(1-n)/n} \right), \quad (4)$$

$$\varepsilon_{\text{EIS}} = \left( \frac{R_{ct(\text{inh})} - R_{ct(\text{bl})}}{R_{ct(\text{inh})}} \right) \times 100\%. \quad (5)$$

The EIS results (Table 4) revealed direct proportionality between CMSE concentrations and inhibition efficiency. This suggests that CMSE acted as a protective layer for carbon steel surface corrosion in the chloride solution [31]. The values of  $n$  revealed the degree of surface homogeneity of the carbon steel in the presence and absence of CMSE. Nonetheless, the polarization resistance  $R_{ct}$  increased from 16.4 to 211.6  $\Omega \text{ cm}^2$  but bilayer capacitance  $C_{dl}$  decreased from 173.7  $\mu\text{F}/\text{cm}^2$  to 48.1  $\mu\text{F}/\text{cm}^2$  as the CMSE concentration was increased from 2 to 10  $\text{g L}^{-1}$ . This suggests CMSE effectiveness in reducing the corrosion rate via film coverage improvement on the A515 Grade 70 carbon steel surface. Also, the result could be associated with electrical double-layer thickness evolution [32].

**3.2. Adsorption Isotherm.** The adsorption nature of CMSE molecules on A515 Grade 70 carbon steel in 1 M NaCl solution at 303 K was determined using Langmuir adsorption

isotherm stated as Equation (6). Previous studies have proved Langmuir isotherm to be the best model for fitting corrosion data [28, 33, 34]. The corrosion inhibition efficiencies calculated using the EIS method was used to evaluate the surface coverage ( $\theta = IE_E/100$ ) presented in Table 5. A plot of  $\log(C/\theta)$  versus  $\log C$  (Figure 4) revealed a correlation coefficient of 0.999 suggesting a monolayer adsorption of CMSE molecules on carbon steel surface in the chloride solution [35].

$$\log \left( \frac{C}{\theta} \right) = \log C - \log K, \quad (6)$$

where  $C$  represents CMSE concentration ( $\text{g L}^{-1}$ ),  $K$  is the adsorption equilibrium constant ( $\text{g}^{-1} \text{ L}$ ), and  $\theta$  is the surface coverage.

Gibbs free energy of adsorption (Equation (7)) was estimated to know the interaction nature (chemisorption or physisorption) between CMSE molecules and A515 Grade 70 carbon steel surface in 1 M NaCl solution at a temperature of 303 K. The value of adsorption equilibrium constant ( $K$ ) was estimated from the intercept of Langmuir isotherm model fit (Figure 4) to be 0.673  $\text{g}^{-1} \text{ L}$ . The Gibbs free energy was found to be -16.41  $\text{kJ mol}^{-1}$ . The absolute value of  $\Delta G_{\text{ads}}^{\circ}$  less than 20  $\text{kJ mol}^{-1}$  strongly suggests adsorption of molecules to be more of physisorption [36]. Also, the negative value suggests adsorption of CMSE molecules onto carbon steel surface to be spontaneous in nature. Thus, the disturbance of adsorbate electronic structure occurred due to electrostatic interaction between CMSE molecules and carbon steel surface [37].

$$\Delta G_{\text{ads}}^{\circ} = -2.303RT \log(C_{\text{solvent}}K), \quad (7)$$

where  $R$  is the universal gas constant (8.314  $\text{J mol}^{-1} \text{ K}^{-1}$ ),  $T$  is the absolute temperature (K),  $C_{\text{solvent}}$  is the water

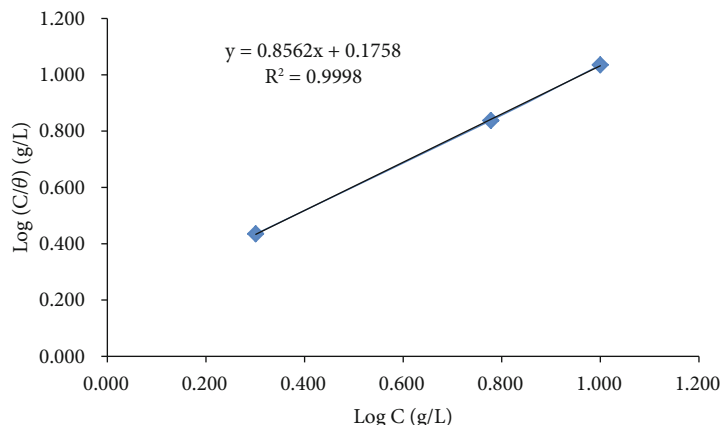


FIGURE 4: Adsorption isotherm plot of carbon steel in in 1 M NaCl solution at 303 K in the absence and presence of various concentrations of CMSE.

TABLE 6: Batch experimental results showing CMSE influence on corrosion rate, yield strength, Young modulus, and hardness of carbon steel in 1.0 M NaCl at different temperature, time, and load.

Run	$T$ ( $^{\circ}\text{C}$ )	$t$ (day)	$C$ ( $\text{g L}^{-1}$ )	Corrosion rate (mm/y)		Load (N)	Young modulus (GPa)		Hardness (BHN)	
				With CMSE	Without CMSE		With CMSE	Without CMSE	With CMSE	Without CMSE
1	30	1	10	0.096	0.306	30000	198.9	187.8	104.1	99
2	60	1	10	0.36	1.211	15000	196.4	189.1	97.2	93.4
3	30	5	10	0.125	0.475	15000	198.7	188.6	106.4	101.6
4	60	5	10	0.516	1.348	30000	180.9	171.7	89.4	86.4
5	45	3	6	0.329	1.587	22500	186.4	178.1	96.1	92.1
6	45	3	6	0.306	0.818	7500	199.5	194.2	100.8	97
7	45	3	14	0.216	0.648	22500	187.4	183.7	99.6	95.7
8	30	5	2	0.197	0.591	15000	193.1	183.2	102.3	97.6
9	30	5	10	0.139	0.417	30000	191.3	183.9	98.7	93.7
10	45	3	2	0.37	1.019	22500	182.6	176.9	95.5	91
11	45	3	6	0.285	0.955	22500	185.6	178.1	98.5	93.8
12	45	3	6	0.351	1.153	37500	179.6	174.4	93.8	89.6
13	45	3	6	0.333	0.882	22500	191.1	178.1	95.8	91.8
14	45	3	6	0.296	0.888	22500	184.8	178.1	97.2	92.6
15	45	3	6	0.309	0.927	22500	183.1	178.1	96.7	92.1
16	15	3	6	0.131	0.593	22500	197.3	194.2	103.8	100.4
17	30	1	10	0.0728	0.218	15000	202.4	194.8	112.3	107.2
18	45	1	6	0.241	0.923	22500	188.2	181.7	97.7	94.3
19	60	1	2	0.604	1.812	30000	176.7	170.4	88.8	86
20	75	3	6	0.388	1.164	22500	181.2	173.8	94.3	91.5
21	30	5	2	0.183	0.549	30000	189.6	180.5	97.9	92.4
22	45	3	6	0.372	1.156	22500	182.6	178.1	94.8	91.1
23	60	1	10	0.389	1.177	30000	178.4	172	92.3	89
24	45	7	6	0.412	1.256	22500	179.7	176.3	93.2	89.1
25	60	5	2	0.733	2.199	15000	184.1	178.7	92.1	87.9
26	30	1	2	0.128	0.364	30000	195.9	188.6	101.1	96.4
27	30	1	2	0.103	0.319	15000	200.8	193.6	109.6	104.3
28	60	5	2	0.781	2.373	30000	174.6	165.9	86.3	84.4
29	60	5	10	0.464	1.692	15000	195.5	186.5	94.4	90.8
30	60	1	2	0.589	1.767	15000	194.3	185.5	93.6	90.3

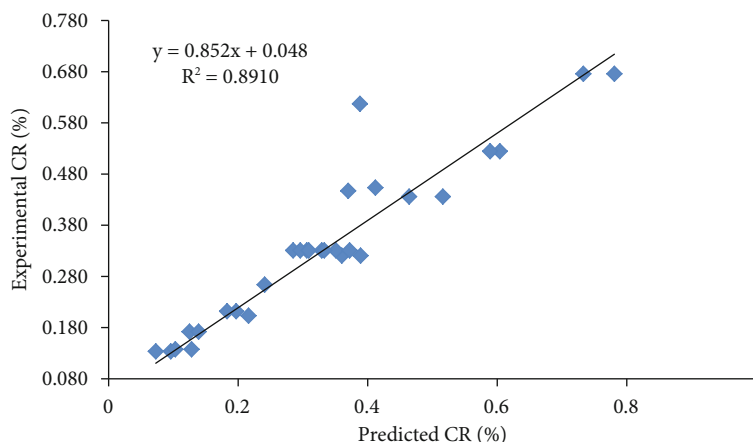


FIGURE 5: Corrosion rate experimental versus predicted values.

TABLE 7: Type III ANOVA result for corrosion rate.

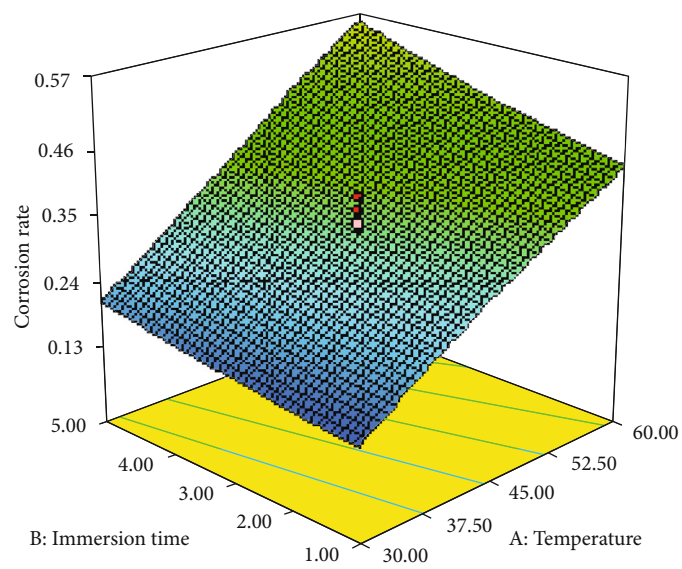
Source	Sum of Squares	df	Mean Square	F value	p value Prob > F	
Model	0.83089	9	0.09232	12.87092	<0.0001	Significant
$X_1$ -temperature	0.63577	1	0.63577	88.63545	<0.0001	
$X_2$ -immersion time	0.05398	1	0.05398	7.52551	0.0125	
$X_3$ -inhibitor concentration	0.08933	1	0.08933	12.45373	0.0021	
$X_1X_2$	0.00592	1	0.00592	0.82552	0.3744	
$X_1X_3$	0.03998	1	0.03998	5.57382	0.0285	
$X_2X_3$	0.00129	1	0.00129	0.18018	0.6757	
$X_1^2$	0.00267	1	0.00267	0.37258	0.5485	
$X_2^2$	0.00136	1	0.00136	0.19021	0.6674	
$X_3^2$	0.00005	1	0.00005	0.00759	0.9314	
Residual	0.14346	20	0.00717			
Lack of fit	0.13366	5	0.02673	0.164891	0.5316	Not significant
Pure error	0.00979	15	0.00065			
Cor. total	0.97434	29				

concentration (1000 g/L), and  $K$  is the adsorption equilibrium constant ( $\text{g}^{-1} \text{L}$ ).

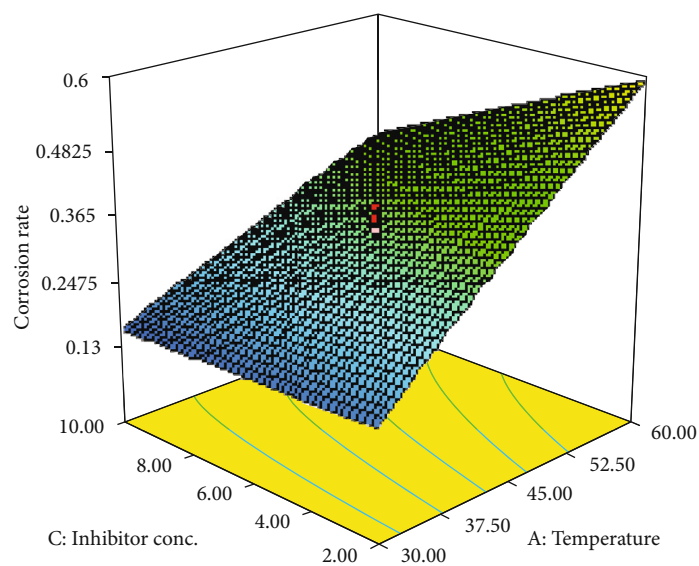
### 3.3. Gravimetric Measurement Batch Corrosion Experiments

**3.3.1. Corrosion Rate Determination.** Table 6 presents the corrosion batch experimental results showing CMSE influence on corrosion rate, Young modulus, and hardness of carbon steel in 1.0 M NaCl at different CMSE concentration, temperature, immersion time, and load. Parameter distribution within the table was generated using the central composite design of Design Expert software. In the presence of CMSE as corrosion inhibitor for the carbon steel in 1.0 M NaCl solution, corrosion rate of 0.0728 mm/y was observed at temperature, immersion time, and CMSE concentration of 30°C, 1 day, and 10 gL<sup>-1</sup>, respectively. At temperature, immersion time, and CMSE concentration of 60°C, 5 days,

and 2 gL<sup>-1</sup>, respectively, corrosion rate of 0.781 mm/y was recorded. At higher temperature, the ions in the carbon steel are energized and thus are liberated from the surface. These are lost into the corrosive medium and thereby increase the weight loss of the carbon steel in 1.0 M NaCl which causes increase in the corrosion rate. Also, the weight loss and corrosion rate increased as the immersion period of carbon steel in the NaCl corrosive medium was increased. High significance of CMSE as corrosion inhibitor for the examined carbon steel coupons manifested in the result obtained. The higher the concentration of corrosion inhibitor, the more the thin films formed on metal steel surface which act as protective layer against corrosion attack in the medium. However, increased in corrosion rate of carbon steel was observed in all the experimental runs conducted in the absence of CMSE as corrosion inhibitor when compared with results obtained in the presence of CMSE. This



(a)



(b)

FIGURE 6: Continued.



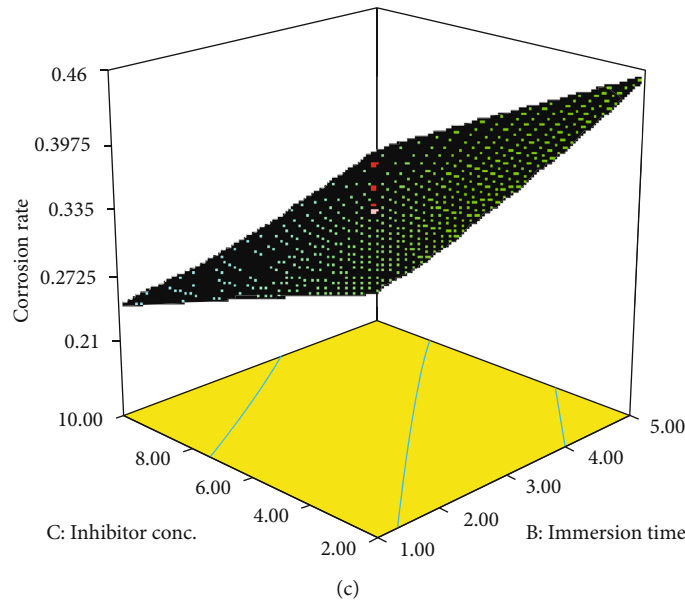


FIGURE 6: 3D response surface plot showing (a) immersion time and temperature (b) inhibitor concentration and temperature and (c) immersion time and inhibitor concentration influence on corrosion rate.

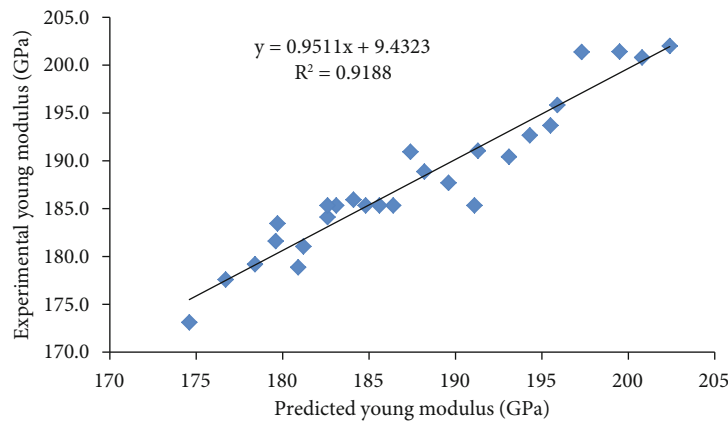


FIGURE 7: Young modulus experimental versus predicted values.

could be linked to the exposure of carbon steel to the corrosive medium without the formation of barriers that could protect it via formation of films by the corrosion inhibitor. The minimum and maximum corrosion rates observed were 0.218 and 2.373 mm/yr. These were also obtained at the same process conditions of temperature and immersion time, as observed in the presence of CMSE in the corrosive medium.

3.3.2. *Model Development and Fitness.* Equation (8) gives the mathematical model developed by the CCD for future prediction of batch corrosion rate of carbon steel in 1.0 M NaCl using CMSE as corrosion inhibitor. Figure 5 gives a correlation plot between experimental and predicted values of corrosion rate with  $R^2$  value of 0.891 suggesting 89.1% of the predicted corrosion rate values could best be described by

the independent variables. The developed model equation could not explain the remaining 10.9%.

$$\begin{aligned}
 \text{CR (mm/y)} = & +0.33 + 0.16X_1 + 0.047X_2 \\
 & - 0.061X_3 + 0.019X_1X_2 - 0.05X_1X_3 \\
 & - 8.987 \times 10^{-3}X_2X_3 - 9.77 \times 10^{-3}X_1^2 \\
 & + 6.98 \times 10^{-3}X_2^2 - 1.395 \times 10^{-3}X_3^2.
 \end{aligned} \tag{8}$$

3.3.3. *Type III ANOVA Analysis.* The result of type III ANOVA, presented in Table 7, revealed the model and variables to be significant. The  $F$  value obtained for the model was approximately 12.87, a  $p$  value of less than 0.0001 signifies the model was exact, and variables were significant to the study. This also justifies that selection of quadratic as process order was significant. The order of variable

TABLE 8: Type III ANOVA result for Young modulus.

Source	Sum of Squares	df	Mean Square	F value	p value Prob > F	
Model	1686.437	14	120.460	11.848	<0.0001	Significant
X <sub>1</sub> -temperature	620.167	1	620.167	60.996	<0.0001	
X <sub>2</sub> -immersion time	133.859	1	133.859	13.166	0.0025	
X <sub>3</sub> -inhibitor concentration	56.567	1	56.567	5.564	0.0323	
X <sub>4</sub> -load	588.060	1	588.060	57.838	<0.0001	
X <sub>1</sub> X <sub>2</sub>	13.323	1	13.323	1.310	0.2703	
X <sub>1</sub> X <sub>3</sub>	5.760	1	5.760	0.567	0.4633	
X <sub>1</sub> X <sub>4</sub>	102.010	1	102.010	10.033	0.0064	
X <sub>2</sub> X <sub>3</sub>	17.223	1	17.223	1.694	0.2127	
X <sub>2</sub> X <sub>4</sub>	5.063	1	5.063	0.498	0.4912	
X <sub>3</sub> X <sub>4</sub>	4.000	1	4.000	0.393	0.5399	
X <sub>1</sub> <sup>2</sup>	61.268	1	61.268	6.026	0.0268	
X <sub>2</sub> <sup>2</sup>	12.235	1	12.235	1.203	0.2900	
X <sub>3</sub> <sup>2</sup>	4.600	1	4.600	0.452	0.5114	
X <sub>4</sub> <sup>2</sup>	67.676	1	67.676	6.656	0.0209	
Residual	152.510	15	10.167			
Lack of fit	105.730	10	10.573	1.130	0.4745	Not significant
Pure error	46.780	5	9.356			
Cor. total	1838.947	29				

significance was temperature > inhibitor concentration > immersion time with approximately  $F$  values of 88.63, 12.45, and 7.53, respectively. Also, the model lack of fit was insignificant relative to pure error with  $F$  value of 0.17.

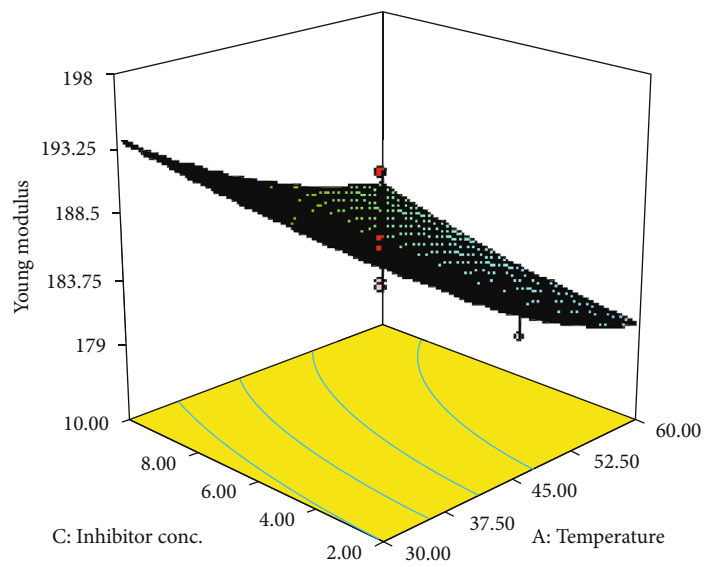
**3.3.4. Response Surface Plot of Parameter Interaction for Corrosion Rate.** The influence of two independent parameters on corrosion rate at constant value of remaining parameter is represented by 3D response surface plots shown in Figure 6. When the inhibitor concentration was kept at a constant value of  $6 \text{ gL}^{-1}$ , a maximum corrosion rate of approximately  $0.57 \text{ mm/y}$  was obtained for combinatory effect of immersion time and temperature (Figure 6(a)). At constant 3 days immersion time, maximum corrosion rate of approximately  $0.6 \text{ mm/y}$  was achieved for combinatory interaction of inhibitor concentration and temperature (Figure 6(b)). Lastly, combinatory effect of inhibitor concentration and immersion time as constant temperature of  $45^\circ\text{C}$  gave maximum corrosion rate of approximately  $0.46 \text{ mm/y}$  (Figure 6(c)). This is a strong indication of high significance of combinatory effect of inhibitor concentration and temperature on corrosion rate of carbon steel in  $1.0 \text{ M NaCl}$  solution.

### 3.4. Young Modulus Experiments

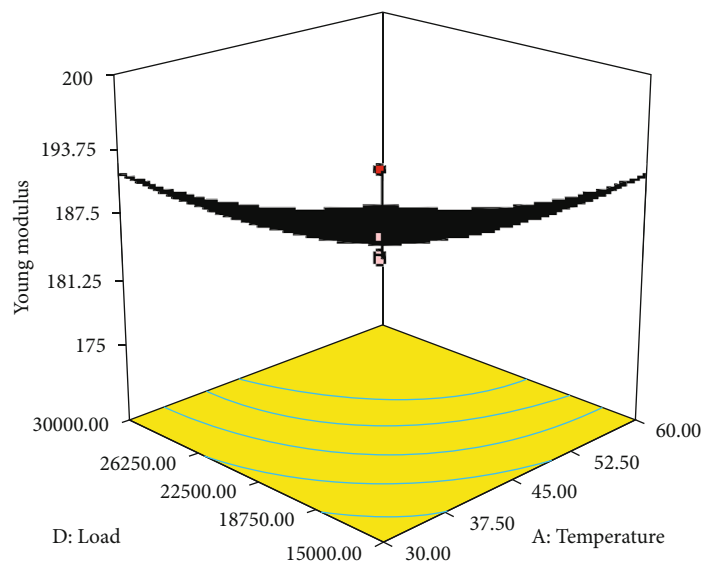
**3.4.1. Determination of Young Modulus.** The Young modulus results, obtained at different corrosion rates of carbon steel coupons subjected to varying loads in the presence and absence of CMSE as corrosion inhibitor in  $1.0 \text{ M NaCl}$  solu-

tion, are presented in Table 6. Central composite design of design expert was used to obtain experimental run conditions at varying parameters. Corrosion rate values were obtained in the presence and absence of CMSE under the same temperature and immersion time. Young modulus of  $202.4 \text{ GPa}$  was recorded for carbon steel coupon with corrosion rate of  $0.0728 \text{ mm/y}$  when subjected to a load of  $15,000 \text{ N}$  in the presence of CMSE. In the absence of CMSE, Young modulus of  $194.8 \text{ GPa}$  was recorded for carbon steel coupon with corrosion rate of  $0.218 \text{ mm/y}$  when subjected to the same load. Also, a Young modulus of  $174.6 \text{ GPa}$  was recorded for carbon steel coupon with corrosion rate of  $0.781 \text{ mm/y}$  when subjected to a load of  $30,000 \text{ N}$  in the presence of CMSE. In the absence of CMSE, Young modulus of  $165.9 \text{ GPa}$  was recorded for carbon steel coupon with corrosion rate of  $2.373 \text{ mm/y}$  when subjected to the same load. The results revealed decrease in Young modulus of carbon steel when subjected to higher load and also under corrosion attack in the absence of CMSE as corrosion inhibitor. Thus, load and CMSE have high significance on the strength of carbon steel. Generally, maximum Young modulus was recorded at minimum corrosion rate and load while minimum Young modulus was recorded at maximum corrosion rate and load. Corrosion rate and load have strong influence on the mechanical strength of carbon steel.

**3.4.2. Model Development and Fitness.** The mathematical model for carbon steel Young modulus prediction in  $1.0 \text{ M NaCl}$  using CMSE as corrosion inhibitor is presented as Equation (9). A correlation plot between experimental and

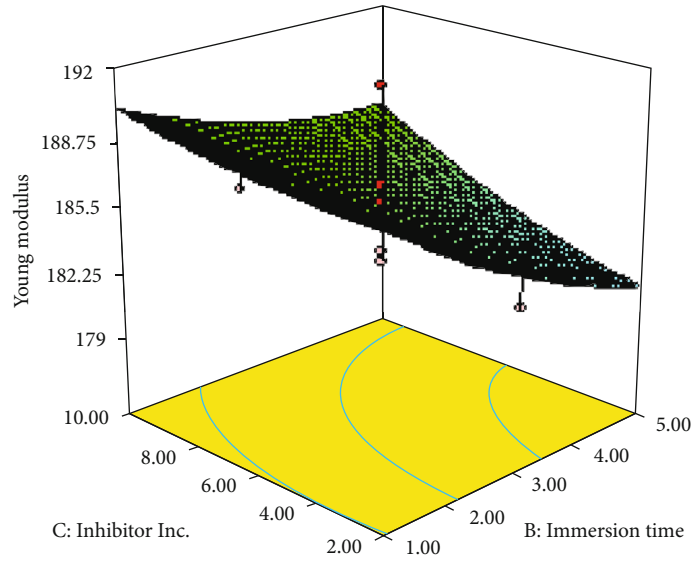


(a)

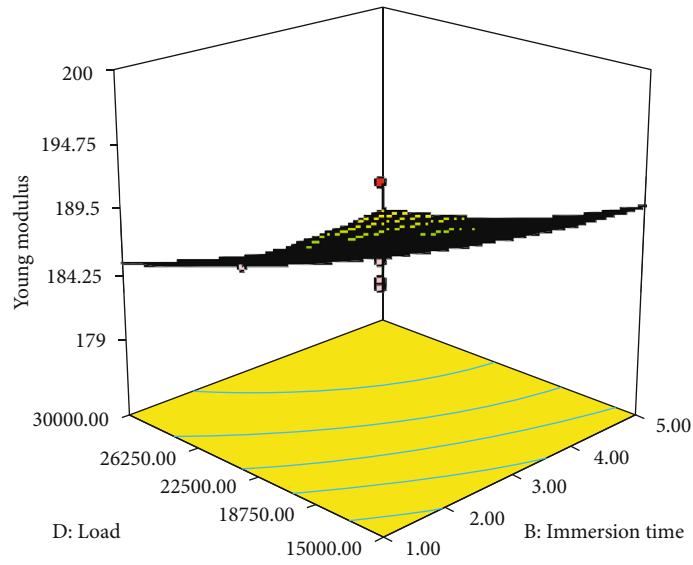


(b)

FIGURE 8: Continued.



(e)



(d)

FIGURE 8: Continued.

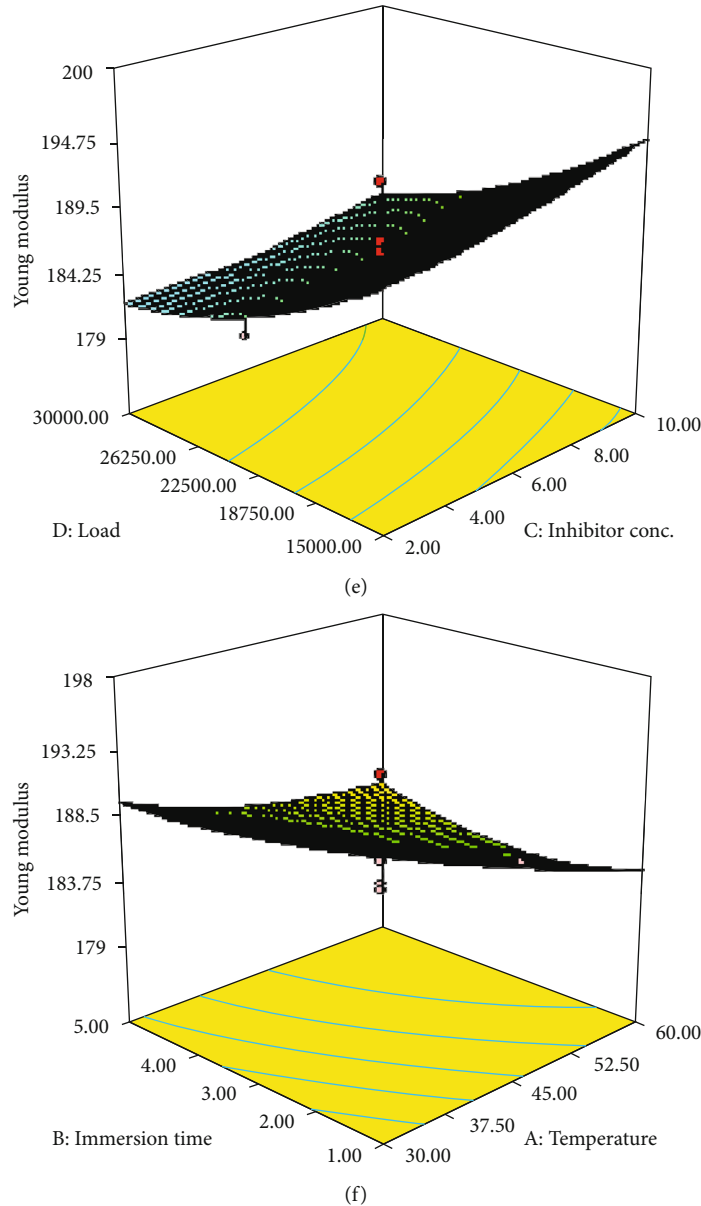


FIGURE 8: 3D response surface plot showing (a) inhibitor concentration and temperature, (b) load and temperature, (c) inhibitor concentration and immersion time, (d) load and immersion time, (e) load and inhibitor concentration, and (f) immersion time and temperature influence on Young Modulus.

predicted values of Young modulus is presented in Figure 7, and  $R^2$  value of 0.918 was obtained. This implies that the independent variables could best describe 91.8% of the values of predicted Young modulus while the remaining 8.2% could not be explained by the developed model equation.

$$\begin{aligned}
 \text{Young Modulus (GPa)} = & +185.33 - 5.08X_1 - 2.68X_2 + 1.74X_3 \\
 & \cdot - 4.95X_4 + 0.91X_1X_2 + 0.60X_1X_3 \\
 & \cdot - 2.53X_1X_4 + 1.04X_2X_3 + 0.56X_2X_4 \quad (9) \\
 & \cdot - 0.50X_3X_4 + 1.47X_1^2 + 0.87X_2^2 \\
 & + 0.53X_3^2 + 1.55X_4^2.
 \end{aligned}$$

3.4.3. Type III ANOVA Analysis. Table 8 presents type III ANOVA result for the Young modulus. The result showed

that both the variables and model were significant. The  $p$  value obtained for the model was less than 0.0001, and its respective  $F$  value was approximately 11.848. This suggests that the model was exact. Also, the variables and selected quadratic (as process order) were significant to the study. The order of variable significance to the Young modulus study was temperature > load > immersion time > inhibitor concentration with approximately  $F$  values of 61, 58, 13, and 6, respectively. Nonetheless,  $F$  value of 0.4745 obtained for the model lack of fit suggests its insignificance relative to pure error.

3.4.4. Response Surface Plot of Parameter Interaction for Young Modulus. The 3D response surface plots showing the influence of two independent parameters on Young

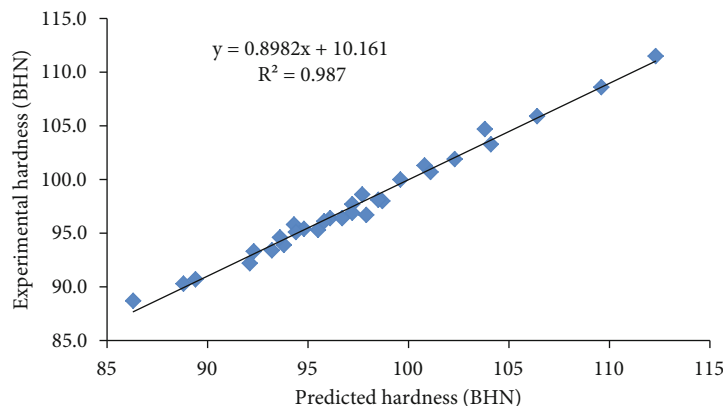


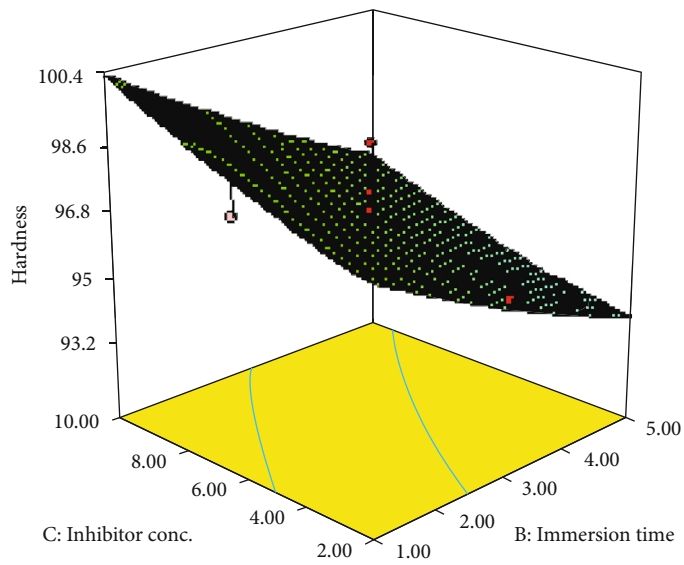
FIGURE 9: Hardness experimental versus predicted values.

TABLE 9: Type III ANOVA result for hardness.

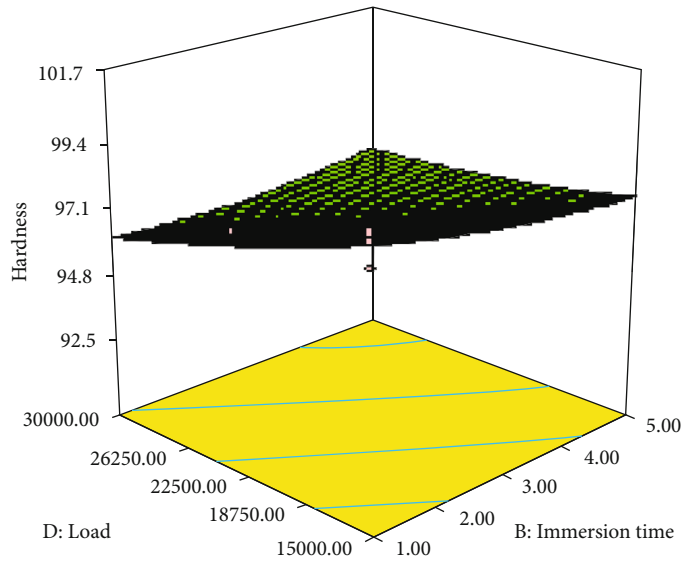
Source	Sum of Squares	df	Mean Square	F value	p value Prob > F	
Model	889.600	14	63.543	9.591	<0.0001	Significant
$X_1$ -temperature	573.304	1	573.304	86.537	<0.0001	
$X_2$ -immersion time	69.921	1	69.921	10.554	0.0054	
$X_3$ -inhibitor concentration	35.326	1	35.326	5.332	0.0356	
$X_4$ -load	166.954	1	166.954	25.201	0.0002	
$X_1X_2$	9.151	1	9.151	1.381	0.2582	
$X_1X_3$	0.226	1	0.226	0.034	0.8561	
$X_1X_4$	4.306	1	4.306	0.650	0.4327	
$X_2X_3$	0.391	1	0.391	0.059	0.8114	
$X_2X_4$	0.766	1	0.766	0.116	0.7386	
$X_3X_4$	0.331	1	0.331	0.050	0.8262	
$X_1^2$	13.910	1	13.910	2.100	0.1679	
$X_2^2$	0.639	1	0.639	0.096	0.7604	
$X_3^2$	0.730	1	0.730	0.110	0.7446	
$X_4^2$	1.964	1	1.964	0.296	0.5941	
Residual	99.374	15	6.625			
Lack of fit	91.306	10	9.131	1.658	0.0348	Not significant
Pure error	8.068	5	1.614			
Cor. total	988.974	29				

modulus while the remaining two parameters are kept constant is presented in Figure 8. At constant values of 3 days and 22,500 N for immersion time and load, respectively, combinatory effect of inhibitor concentration and temperature yielded a maximum Young modulus of approximately 193 GPa (Figure 8(a)). At constant values of 3 days immersion time and 6 gL<sup>-1</sup> inhibitor concentration, a maximum Young modulus of approximately 190 GPa was obtained for the combinatory effect of load and temperature (Figure 8(b)). At constant values of 45°C and 22,500 N for temperature and load, respectively, combinatory effect of inhibitor concentration and time gave a maximum Young

modulus of approximately 189 GPa (Figure 8(c)). At constant values of 45°C temperature and 6 gL<sup>-1</sup> inhibitor concentration, a maximum Young modulus of approximately 185 GPa was obtained for the combinatory effect of load and immersion time (Figure 8(d)). An approximate Young modulus of 181 GPa was obtained for the combinatory effect of load and inhibitor concentration at constant values of 45°C temperature and 3 days immersion time (Figure 8(e)). Lastly, combinatory effect of immersion time and temperature gave Young modulus of approximately 189 GPa at constant values of 6 gL<sup>-1</sup> inhibitor concentration and 22,500 N load (Figure 8(f)). In conclusion, this suggests

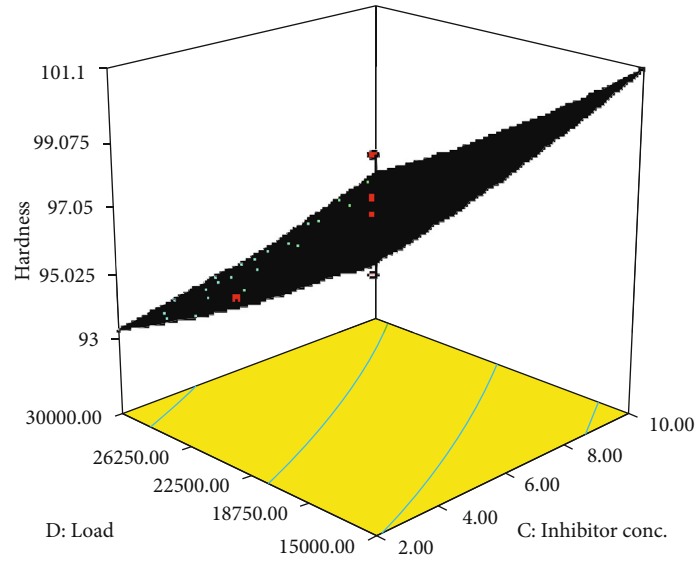


(a)

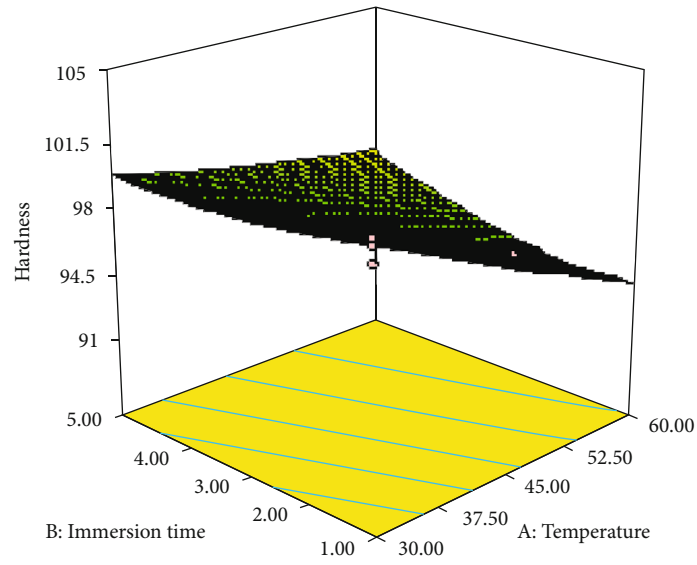


(b)

FIGURE 10: Continued.



(e)



(d)

FIGURE 10: Continued.



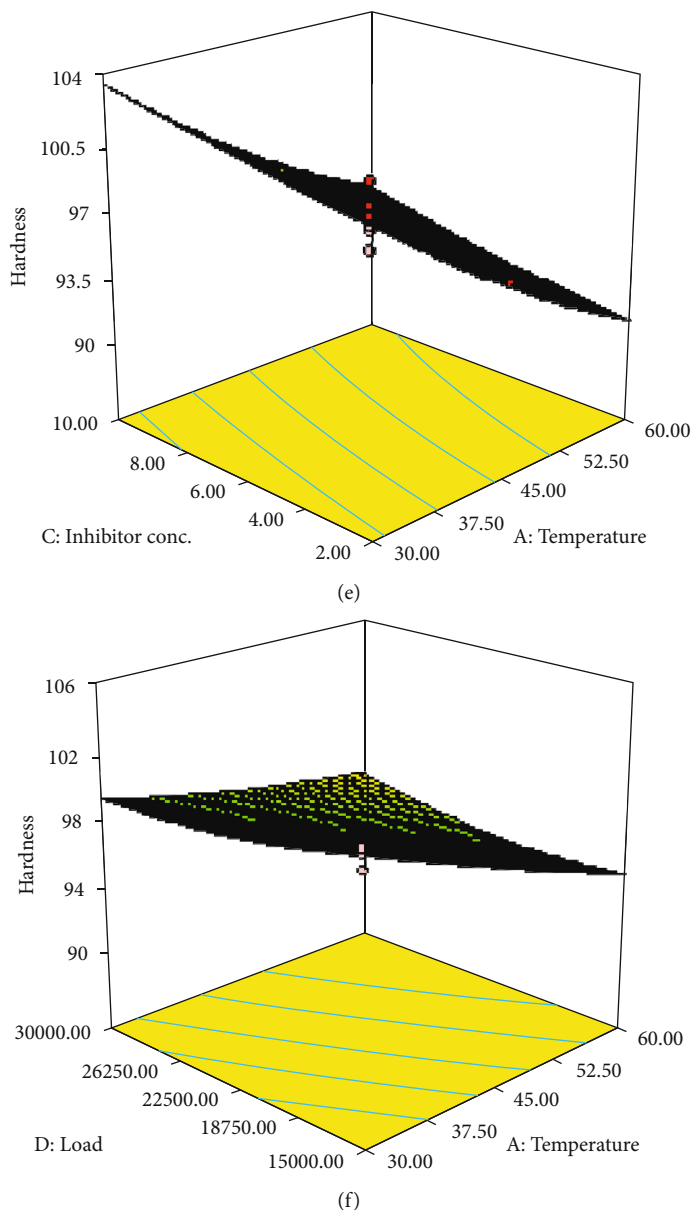


FIGURE 10: 3D response surface plot showing (a) inhibitor concentration and immersion time, (b) load and immersion time, (c) load and inhibitor concentration, (d) immersion time and temperature, (e) inhibitor concentration and temperature, and (f) load and temperature influence on hardness.

TABLE 10: Optimum point prediction by Box-Behnken Design and experimental result at optimum predicted point.

Parameter	Optimum predicted value	Corrosion rate (mm/y)		Young modulus (GPa)		Hardness (BHN)	
		Pred.	Exp.	Pred.	Exp.	Pred.	Exp.
Temperature ( $X_1$ )	32.09°C	0.141	0.137	193.81	192.16	103.07	104.48
Immersion time ( $X_2$ )	1.23 day	—	—				
Inhibitor concentration ( $X_3$ )	7.08 g L <sup>-1</sup>	—	—				
Load ( $X_4$ )	24,646.50 N	—	—				

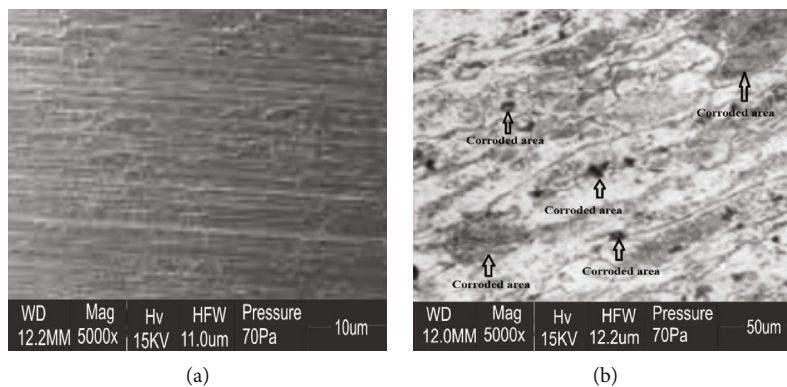


FIGURE 11: SEM surface morphology of A515 Grade 70 CS in 1.0 M HCl for 5 days at temperature 60°C with magnification of  $\times 5000$  in the (a) presence of  $10 \text{ g L}^{-1}$  CMSE and (b) absence of CMSE.

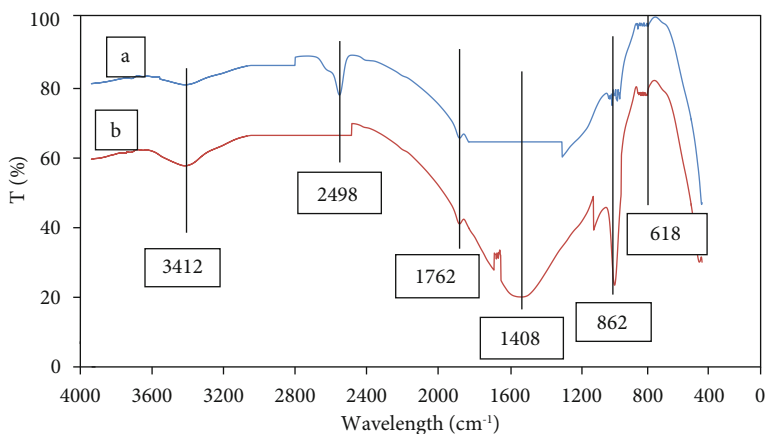


FIGURE 12: FTIR spectra of (a) *Cucumeropsis mannii* shell extract and (b) adsorbed film on A515 Grade 70 CS surface.

TABLE 11:  $\text{Fe}^{2+}$  concentration loss during corrosion experiments with and without CMSE.

Immersion time (day)	$\text{Fe}^{2+}$ conc. (ppm) in solution	
	Without CMSE	With CMSE
1	0.13	0.009
2	0.19	0.013
3	0.28	0.026
4	0.44	0.038
5	0.59	0.044

high significance of inhibitor concentration and temperature combinatory effect on Young modulus of carbon steel in 1.0 M NaCl solution.

### 3.5. Hardness Test

**3.5.1. Determination of Hardness.** The hardness results for carbon steel coupons examined under different loads at different corrosion rates in the corrosive medium with and without

CMSE are presented in Table 6. At a corrosion rate of 0.0728 mm/y when the carbon steel was under a load of 15,000 N in the presence of CMSE, the coupon recorded hardness of 112.3 BHN. At a corrosion rate of 0.218 mm/y when the carbon steel was under the same load in the absence of CMSE, the coupon recorded hardness of 107.2 BHN. Under a load of 30,000 N, hardness of 86.3 and 84.4 BHN was recorded for the carbon steel at corrosion rates of 0.781 and 2.373 mm/y in the presence and absence of CMSE, respectively. A decrease in the hardness of carbon steel was observed under higher load and also when subjected to corrosion attack in the absence of CMSE as corrosion inhibitor. Thus, load and CMSE strongly affect carbon steel hardness. Generally, maximum hardness was recorded at minimum corrosion rate and load while minimum hardness was recorded at maximum corrosion rate and load.

**3.5.2. Model Development and Fitness.** Equation (10) represents mathematical model for the prediction of carbon steel hardness in 1.0 M NaCl using CMSE as corrosion inhibitor. Figure 9 presents the correlation plot between experimental and predicted values of hardness with  $R^2$  value of 0.987. This

TABLE 12: Chemical composition of A515 Grade 70 CS with and without CMSE.

Material	Element compositions (%)							
	Fe	C	Mn	P	Si	S	Cl	O
A515 Grade 70 CS (coupon)	98.00	0.35	1.20	0.035	0.375	0.040	—	—
A515 Grade 70 CS (with CMSE)	93.61	0.28	1.11	0.031	0.351	0.032	0.396	4.19
A515 Grade 70 CS (without CMSE)	80.77	0.19	1.03	0.026	0.333	0.028	2.073	15.55

indicates that the independent variables could best describe 98.7% of the values of predicted hardness while the remaining 1.3% could not be explained by the developed model equation.

$$\begin{aligned}
 \text{Hardness (BHN)} = & +96.44 - 4.89X_1 - 1.93X_2 + 1.38X_3 \\
 & - 2.64X_4 + 0.76X_1X_2 + 0.12X_1X_3 \\
 & + 0.52X_1X_4 - 0.16X_2X_3 + 0.22X_2X_4 \\
 & - 0.14X_3X_4 + 0.7X_1^2 + 0.2X_2^2 + 0.21X_3^2 \\
 & + 0.26X_4^2.
 \end{aligned} \tag{10}$$

**3.5.3. Type III ANOVA Analysis.** Type III ANOVA result of the hardness test for carbon steel is presented in Table 9. All the examined variables and model were significant to the study.  $F$  value of the model was 9.591 while its respective  $p$  value was less than 0.0001 suggesting the model exactness. The order of variable significance to the hardness study was temperature > load > immersion time > inhibitor concentration with approximately  $F$  values of 87, 25, 11, and 5, respectively. Nonetheless,  $F$  value of 1.658 obtained for the model lack of fit suggests its insignificance relative to pure error.

**3.5.4. Response Surface Plot of Parameters Interaction for Hardness.** Figure 10 presents 3D response surface plots of two independent parameters influence on hardness while keeping the remaining two parameters constant. At constant values of 45°C and 22,500 N for temperature and load, respectively, maximum hardness of approximately 100 BHN was recorded for combinatory effect of inhibitor concentration and immersion time (Figure 10(a)). At constant values of 45°C temperature and 6 gL<sup>-1</sup> inhibitor concentration, a maximum hardness of approximately 96 BHN was exhibited for the combinatory effect of load and immersion time (Figure 10(b)). Combinatory effect of inhibitor concentration and load gave a maximum hardness of approximately 93 BHN (Figure 10(c)) at constant values of 45°C and 3 days for temperature and immersion time, respectively. When inhibitor concentration and load were kept at 6 gL<sup>-1</sup> and 22,500 N, respectively, a maximum hardness of approximately 98 BHN was obtained for the combinatory effect of immersion time and temperature (Figure 10(d)). An approximate hardness of 103 BHN was obtained for the combinatory effect of temperature and inhibitor concentration at constant values of 22,500 N load and 3 days immersion time (Figure 10(e)). Lastly, combinatory effect of load and temperature gave hardness of approximately 99 BHN at constant values of 6 gL<sup>-1</sup>

inhibitor concentration and 3 days immersion time (Figure 10(f)). Conclusively, inhibitor concentration and temperature gave the highest combinatory effect on the hardness of carbon steel in 1.0 M NaCl solution.

**3.6. Optimum Point Prediction.** The optimum predicted values for temperature, immersion time, inhibitor concentration, and load were 32.59°C, 1.23 day, 7.08 gL<sup>-1</sup>, and 24,646.50 N, respectively, for A515 Grade 70 carbon steel in NaCl solution using CMSE as corrosion inhibitor. The predicted and experimental values obtained at this optimum point for corrosion rate, Young modulus, and hardness were 0.141 and 0.137 mm/y, 193.81 and 192.16 GPa, and 103.07 and 104.48 BHN, respectively, as presented in Table 10. Small relative errors between the predicted and experimental values suggested (1) better mathematical model with excellent correlation for future prediction and (2) effectiveness of CMSE as excellent corrosion inhibitor for A515 Grade 70 carbon steel in NaCl solution.

### 3.7. Characterization

**3.7.1. Surface Morphology Analysis.** The surface morphology of A515 Grade 70 CS when exposed to 1.0 M NaCl solution for 5 days of immersion at 60°C in the presence and absence of CMSE is presented in Figures 11(a) and 11(b), respectively. The surface of A515 Grade 70 CS in the presence of 10 gL<sup>-1</sup> CMSE revealed a relatively smooth surface with deposited extract of CMS. This resulted from the formation of adsorbed protective film on the surface which acted as a barrier between A515 Grade 70 CS and chloride salt solution. However, at the same magnification, A515 Grade 70 CS was seen to be seriously attacked by uniform [2] and pitting [38] corrosion when immersed in chloride solution without CMSE under the same operating conditions.

**3.7.2. Fourier Transform Infrared Spectroscopy Analysis.** Figure 12 depicts the FTIR spectra of CMSE and adsorbed film on A515 Grade 70 CS surface. In both, absorption bands observed at 3412 cm<sup>-1</sup>, 1762 cm<sup>-1</sup>, 862 cm<sup>-1</sup>, and 618 cm<sup>-1</sup> are related to stretching vibrations of -OH group (which is a strong indication of water molecules presence) [39], strong C=O stretching [40], strong C-Cl stretching [41], and out-of-plane vibration bands of Al-O [42], respectively. Absorption band observed at 2498 cm<sup>-1</sup> on CMSE FTIR spectrum (Figure 12(a)) could be ascribed to strong O=C=O stretching [43] while the absorption band observed at 1408 cm<sup>-1</sup> on the spectrum of adsorbed film on A515 Grade 70 CS surface (Figure 12(b)) was due to medium C-H bending vibration [44].

**3.7.3. Atomic Adsorption Spectroscopy Analysis.** The concentration of  $\text{Fe}^{2+}$  loss into the corrosive medium increased drastically from 0.13 ppm to 0.59 ppm during corrosion experiments conducted without CMSE at 60°C between immersion periods of 1 to 5 days as revealed by AAS analysis (Table 11). However, a gradual increase in the concentration of  $\text{Fe}^{2+}$  loss into 1.0 M NaCl from 0.009 ppm to 0.044 ppm within the same immersion periods and temperature in the presence of 10 g L<sup>-1</sup> CMSE justifies its high significance in inhibiting the corrosion of A515 Grade 70 CS. Loss of  $\text{Fe}^{2+}$  resulted from the corrosive attack by the chloride solution. A strong bond between molecules of CMSE and  $\text{Fe}^{2+}$  reduced its loss into solution during the corrosion experiment conducted.

**3.7.4. Energy Dispersive Spectroscopy Analysis.** The chemical composition of iron present in the A515 Grade 70 CS reduced from 98% to 93.61% and 80.77% while carbon reduced from 0.35% to 0.28% and 0.19% in the presence and absence of CMSE, respectively, when examined in 1.0 M NaCl at 60°C for 5 days as shown by EDS result presented in Table 12. The loss of iron and carbon into solution resulted from corrosion attack by the chloride salt. High rate of A515 Grade 70 CS corrosion in the absence of CMSE was evident in the percentage of oxygen present on the surface (15.55%). This enhances the oxidation of ferrous hydroxide into magnetite, a major significance of uniform and pitting corrosion. The presence of thin film on A515 Grade 70 CS surface prevents oxidation to occur, and thus 4.19% of oxygen was recorded in the presence of 10 g L<sup>-1</sup> CMSE.

## 4. Conclusions

The corrosion inhibition capacity of extract from *Cucumeropsis mannii* shell on A515 Grade 70 carbon steel in NaCl solution has been investigated using potentiodynamic polarization, electrochemical impedance spectroscopy, and weight loss measurements. Maximum inhibition efficiency of 91.2% and 92.2% was recorded for potentiodynamic polarization and electrochemical impedance spectroscopy measurements, respectively. Current density decreased with increasing CMSE concentration while the inhibitor was a mixed type. Polarization resistance increased with increasing inhibitor concentration. The inhibition efficiency increased with increase in CMSE concentration. Adsorption of CMSE molecules on the carbon steel surface in the corrosive medium was monolayer, spontaneous, and physisorption in nature. Corrosion rate decreased as CMSE concentration was increased at lower immersion time and temperature. Maximum Young modulus and hardness were recorded at minimum corrosion rate and load and vice versa. Pitting and uniform corrosion were formed on the carbon steel when tested in NaCl solution without CMSE. Films of protective layer on carbon steel in the presence of CMSE were found to have -OH, -OCH<sub>3</sub>, and -C-NH<sub>3</sub> as active functional groups. In conclusion, *Cucumeropsis mannii* shell extract acted excellently as corrosion inhibitor for A515 Grade 70 carbon steel in 1.0 M NaCl.

## Data Availability

The data used to support the findings of this study are included within the article.

## Conflicts of Interest

The authors declare that they have no conflicts of interest.

## References

- [1] S. Z. Salleh, A. H. Yusoff, S. K. Zakaria et al., "Plant extracts as green corrosion inhibitor for ferrous metal alloys: a review," *Journal of Cleaner Production*, vol. 304, article 127030, 2021.
- [2] I. Saefuloh, N. Kanani, F. G. Ramadhan et al., "The study of corrosion behavior and hardness of AISI stainless steel 304 in concentration of chloride acid solution and temperature variations," *Journal of Physics: Conference Series*, vol. 1477, no. 5, article 052058, 2020.
- [3] Y. Liu, Z. Song, W. Wang et al., "Effect of ginger extract as green inhibitor on chloride-induced corrosion of carbon steel in simulated concrete pore solutions," *Journal of Cleaner Production*, vol. 214, pp. 298–307, 2019.
- [4] B. R. Fazal, T. Becker, B. Kinsella, and K. Lepkova, "A review of plant extracts as green corrosion inhibitors for CO<sub>2</sub> corrosion of carbon steel," *npj Materials Degradation*, vol. 6, 2022.
- [5] M. M. Muzakir, F. O. Nwosub, and S. O. Amusa, "Mild steel corrosion inhibition in a NaCl solution by lignin extract of *Chromolaena odorata*," *Portugaliae Electrochimica Acta*, vol. 37, no. 6, pp. 359–372, 2019.
- [6] W. C. Lyons, G. J. Plisga, and M. D. Lorenz, *Standard Handbook of Petroleum and Natural Gas Engineering*, Elsevier, Amsterdam, 2016.
- [7] C. Thamaraiselvan, N. Michael, and Y. Oren, "Selective separation of dyes and brine recovery from textile wastewater by nanofiltration membranes," *Chemical Engineering and Technology*, vol. 41, no. 2, pp. 185–293, 2018.
- [8] A. Zakeri, E. Bahmani, and A. S. R. Aghdam, "Plant extracts as sustainable and green corrosion inhibitors for protection of ferrous metals in corrosive media: A mini review," *Corrosion Communications*, vol. 5, pp. 25–38, 2022.
- [9] L. T. Popoola, "Corrosion inhibitory effect of mixed cocoa pod-Ficus exasperata extract on MS in 1.5 M HCl: optimization and electrochemical study," *Corrosion Reviews*, vol. 39, no. 2, pp. 109–122, 2021.
- [10] L. Chen, D. Lu, and Y. Zhang, "Organic compounds as corrosion inhibitors for carbon steel in HCl solution: a comprehensive review," *Materials*, vol. 15, no. 6, p. 2023, 2022.
- [11] A. M. Abdel-Karim and A. M. El-Shamy, "A review on green corrosion inhibitors for protection of archeological metal artifacts," *Journal of Bio- and Tribo-Corrosion*, vol. 8, no. 2, p. 35, 2022.
- [12] L. T. Popoola, "Organic green corrosion inhibitors (OGCIs): a critical review," *Corrosion Reviews*, vol. 37, no. 2, pp. 71–102, 2019.
- [13] M. Sangeetha, S. Rajendran, and J. Sathiyabama, "Asafoetida extract as green corrosion inhibitor for mild steel in sea water," *International Research Journal of Environmental Sciences*, vol. 1, pp. 14–21, 2012.
- [14] A. Pradityana, S. A. Shahab, L. Noerochim, and D. Susanti, "Inhibition of corrosion of carbon steel in 3.5% NaCl solution

- by Myrmecodia Pendans extract,” *International Journal of Corrosion*, vol. 2016, Article ID 6058286, 6 pages, 2016.
- [15] S. P. Palanisamy, G. Maheswaran, A. G. Selvarani, C. Kamal, and G. Venkatesh, “\_Ricinus communis\_ - A green extract for the improvement of anti-corrosion and mechanical properties of reinforcing steel in concrete in chloride media,” *Journal of Building Engineering*, vol. 19, pp. 376–383, 2018.
- [16] M. Barbouchi, B. Benzidia, A. Aouidate, A. Ghaleb, M. El-Idrissi, and M. Choukrad, “Theoretical modeling and experimental studies of terebinth extracts as green corrosion inhibitor for iron in 3% NaCl medium,” *Journal of King Saud University-Science*, vol. 32, no. 7, pp. 2995–3004, 2020.
- [17] I. K. Ibrahim and J. A. Naser, “Corrosion inhibition of carbon steel in sodium chloride solution using artemisia plant extract,” *Plant Archives*, vol. 20, no. 1, pp. 3315–3319, 2020.
- [18] V. Vorobyova and M. Skiba, “Peach pomace extract as novel cost-effective and high-performance green inhibitor for mild steel corrosion in NaCl solution: experimental and theoretical research,” *Waste and Biomass Valorization*, vol. 12, no. 8, pp. 4623–4641, 2021.
- [19] M. Dauda, L. S. Kuburi, E. C. Okereke, and A. A. Alabi, “Stress corrosion study of mild steel in acidic media,” *International Journal of Innovative Research in Advanced Engineering*, vol. 6, no. 2, pp. 190–194, 2015.
- [20] Y. Yetri, A. Gunawarman, R. Hidayati, and A. Zamri, “Mechanical properties of mild steel by adding Theobroma Cacao peels extract (TCPE) inhibitor,” *IOP Conference Series: Materials Science and Engineering*, vol. 602, no. 1, article 012088, 2019.
- [21] L. Guo, J. Tan, S. Kaya, S. Leng, Q. Li, and F. Zhang, “Multidimensional insights into the corrosion inhibition of 3,3-dithiodipropionic acid on Q235 steel in H<sub>2</sub>SO<sub>4</sub> medium: a combined experimental and in silico investigation,” *Journal of Colloid and Interface Science*, vol. 570, pp. 116–124, 2020.
- [22] B. Tan, W. Lan, S. Zhang et al., “Passiflora edulia Sims leaves extract as renewable and degradable inhibitor for copper in sulfuric acid solution,” *Colloids and Surfaces A: Physicochemical and Engineering Aspects*, vol. 645, article 128892, 2022.
- [23] S. Mallek-Ayadi, N. Bahloul, and N. Kechaou, “Chemical composition and bioactive compounds of \_Cucumis melo\_ L. seeds: potential source for new trends of plant oils,” *Process Safety and Environmental Protection*, vol. 113, pp. 68–77, 2018.
- [24] M. Afrokh, S. Baroud, Y. Kerroum et al., “Green approach to corrosion inhibition of carbon steel by Fucus spiralis extract in 1 M HCl medium,” *Biointerface Research in Applied Chemistry*, vol. 12, no. 5, pp. 7075–7091, 2021.
- [25] M. A. El-Hashemy and A. Sallam, “The inhibitive action of \_Calendula officinalis\_ flower heads extract for mild steel corrosion in 1 M HCl solution,” *Journal of Materials Research and Technology*, vol. 9, no. 6, pp. 13509–13523, 2020.
- [26] M. El Faydy, R. Touir, M. Ebn Touhami et al., “Corrosion inhibition performance of newly synthesized 5-alkoxymethyl-8-hydroxyquinoline derivatives for carbon steel in 1 M HCl solution: experimental, DFT and Monte Carlo simulation studies,” *Physical Chemistry Chemical Physics*, vol. 20, no. 30, pp. 20167–20187, 2018.
- [27] M. H. Nazari, M. S. Shihab, L. Cao, E. A. Havens, and X. Shi, “A peony-leaves-derived liquid corrosion inhibitor: protecting carbon steel from NaCl,” *Green Chemistry Letters and Reviews*, vol. 10, no. 4, pp. 359–379, 2017.
- [28] M. H. Nazari, M. S. Shihab, E. A. Havens, and X. Shi, “Mechanism of corrosion protection in chloride solution by an apple-based green inhibitor: experimental and theoretical studies,” *Journal of Infrastructure Preservation and Resilience*, vol. 1, no. 1, p. 7, 2020.
- [29] Y. Kerroum, A. Guenbour, A. Bellaouchou, H. Idrissi, J. Garcia-Anton, and A. Zarrouk, “Chemical and physical effects of fluoride on the corrosion of austenitic stainless steel in polluted phosphoric acid,” *Journal of Bio- and Tribo-Corrosion*, vol. 5, no. 3, p. 68, 2019.
- [30] S. J. H. M. Jessima, A. Berisha, S. S. Srikandan, and S. Subhashini, “Preparation, characterization, and evaluation of corrosion inhibition efficiency of sodium lauryl sulfate modified chitosan for mild steel in the acid pickling process,” *Journal of Molecular Liquids*, vol. 320, p. 114382, 2020.
- [31] R. T. Loto and O. Olowoyo, “Synergistic effect of sage and jojoba oil extracts on the corrosion inhibition of mild steel in dilute acid solution,” *Procedia Manufacturing*, vol. 35, pp. 310–314, 2019.
- [32] M. G. Hosseini, M. Ehteshamzadeh, and T. Shahrabi, “Protection of mild steel corrosion with schiff bases in 0.5M H<sub>2</sub>SO<sub>4</sub> solution,” *Electrochimica Acta*, vol. 52, no. 11, pp. 3680–3685, 2007.
- [33] J. T. Nwabanne and V. N. Okafor, “Adsorption and thermodynamics study of the inhibition of corrosion of mild steel in H<sub>2</sub>SO<sub>4</sub> medium using Vernonia Amygdalina,” *Journal of Minerals and Materials Characterization and Engineering*, vol. 11, no. 9, pp. 885–890, 2012.
- [34] L. T. Popoola, “Adsorption and corrosion inhibitive properties of Oryza glaberrima husk extract on aluminium in H<sub>2</sub>SO<sub>4</sub> solution: isotherm, kinetic and thermodynamic studies,” *Studia ubb chemia*, vol. 65, no. 4, pp. 177–201, 2020.
- [35] V. S. Markin, M. I. Volkova-Gugeshashvili, and A. G. Volkov, “Adsorption at liquid interfaces: the generalized Langmuir isotherm and interfacial structure,” *The Journal of Physical Chemistry B*, vol. 110, no. 23, pp. 11415–11420, 2006.
- [36] H. L. Y. Sin, A. Abdul Rahim, C. Y. Gan, B. Saad, M. I. Salleh, and M. Umeda, “\_Aquilaria subintergra\_ leaves extracts as sustainable mild steel corrosion inhibitors in HCl,” *Measurement*, vol. 109, pp. 334–345, 2017.
- [37] M. S. Shihab and A. F. Mahmood, “Experimental and theoretical study of some N-pyridinium salt derivatives as corrosion inhibitors for mild-steel in 1 M H<sub>2</sub>SO<sub>4</sub>,” *Portugaliae Electrochimica Acta*, vol. 35, no. 6, pp. 39–51, 2017.
- [38] S. A. Umoren, I. B. Obot, and N. O. Obi-Egbedi, “Corrosion inhibition and adsorption behaviour for aluminium by extract of aningeriarobusta in HCl solution: synergistic effect of iodide ions,” *Journal of Materials and Environmental Science*, vol. 2, pp. 60–71, 2011.
- [39] S. Ahmed, J. Pan, M. N. Ashiq, D. Li, P. Tang, and Y. Feng, “Ethylene glycol-assisted fabrication and superb adsorption capacity of hierarchical porous flower-like magnesium oxide microspheres for phosphate,” *Inorganic Chemistry Frontiers*, vol. 6, no. 8, pp. 1952–1961, 2019.
- [40] A. S. Yusuff and I. I. Olateju, “Experimental investigation of adsorption capacity of anthill in the removal of heavy metals from aqueous solution,” *Environmental Quality Management*, vol. 13, pp. 53–59, 2018.
- [41] T. H. Kim, V. Rodríguez-González, G. Gyawali, S. H. Cho, T. Sekino, and S. W. Lee, “Synthesis of solar light responsive

- Fe, N co-doped TiO<sub>2</sub> photocatalyst by sonochemical method,” *Catalysis Today*, vol. 212, pp. 75–80, 2013.
- [42] M. Hassani, G. D. Najafpour, M. Mohammadi, and M. Rabiee, “Preparation, characterization and application of zeolite-based catalyst for production of biodiesel from waste cooking oil,” *Journal of Scientific and Industrial Research*, vol. 73, pp. 129–133, 2014.
- [43] Y. He, R. Wang, C. Sun et al., “Facile synthesis of self-assembled NiFe layered double hydroxide-based azobenzene composite films with photoisomerization and chemical gas sensor performances,” *ACS Omega*, vol. 5, no. 7, pp. 3689–3698, 2020.
- [44] R. B. Vignesh, J. Balaji, and M. Sethuraman, “Surface modification, characterization and corrosion protection of 1,3-diphenylthiourea doped sol-gel coating on aluminium,” *Progress in Organic Coating*, vol. 111, pp. 112–123, 2017.